

1 Supplementary material

2

3 **Title: Acidification in coastal waters of Adélie Land, Antarctica (1985-2025)**

4

5 Nicolas Metzl¹, Bronte Tilbrook^{2,3}, John Akl², Craig Neill², Alexandra Aymard¹, Claire Lo Monaco¹,
6 Gilles Reverdin¹, Jean-Baptiste Sallée¹, Aude Barton⁴, Frédéric Chevallier⁴, Marion Gehlen⁴

7

8 1 Laboratoire LOCEAN/IPSL, Sorbonne Université-CNRS-IRD-MNHN, Paris, 75005, France

9 2 CSIRO Environment, Castray Esplanade, Hobart, TAS 7004, Australia

10 3 Australian Antarctic Partnership Program, University of Tasmania, Hobart, TAS, Australia

11 4 Laboratoire LSCE/IPSL, CEA-CNRS-UVSQ, Université Paris-Saclay Gif-sur-Yvette, 91191, France

12

13 Correspondence to: Nicolas Metzl (nicolas.metzl@locean.ipsl.fr)

14

15 This document includes Table S1-S2 and Figures S1-S14 providing the supplementary information
16 that supports part of the discussion presented in the main article.

17

18
19
20
21
22
23
24
25
26
27
28
29
30
31
32
33
34
35
36
37
38
39
40
41
42
43
44
45
46
47
48
49
50
51
52
53
54
55
56
57
58
59
60
61
62
63
64
65
66
67
68
69
70
71
72
73

Table S1: List of cruises in the region south of 60°S from SOCAT-v2025 (Bakker et al, 2025) and new data in 2025.

EXPOCODE	Year	Month	Ship	Principal Investigator	Flag
49HH19831123	1984	1	Hakuho Maru	Inoue, H.	D
09AR19910926	1991	10	Aurora Australis	Tilbrook, B.	B
09AR19930311	1993	3	Aurora Australis	Tilbrook, B.	C
09AR19940101	1994	1	Aurora Australis	Tilbrook, B.	B
49HH19941123	1994	12	Hakuho Maru	Inoue, H.	D
09AR19941213	1995	1	Aurora Australis	Tilbrook, B.	B
320619950317	1995	3	Nath. B. Palmer	Takahashi, T. : Sweeney, C. : Sutherland, S.C.	D
09AR19950717	1995	7	Aurora Australis	Tilbrook, B.	B
09AR19950916	1995	9	Aurora Australis	Tilbrook, B.	C
09AR19960119	1996	3	Aurora Australis	Tilbrook, B.	C
09AR19960822	1996	8	Aurora Australis	Tilbrook, B.	C
353L19961021	1996	10	L_Astrolabe	Metzl, N.	D
353L19970202	1997	2	L_Astrolabe	Metzl, N.	D
09AR19980715	1998		Aurora Australis	Tilbrook, B.	B
61TG19990202	1999	2	Tangaroa	Bakker, D.	D
09AR19990716	1999	8	Aurora Australis	Tilbrook, B.	B
320620001220	2000	12	Nath. B. Palmer	Takahashi, T. : Sweeney, C. : Sutherland, S.C.	D
320620010130	2001	2	Nath. B. Palmer	Takahashi, T. : Sweeney, C. : Sutherland, S.C.	B
09AR20011031	2001	10	Aurora Australis	Tilbrook, B.	B
49HH20011128	2002	1	Hakuho Maru	Inoue, H.	D
35MF20030126*	2003	2	Marion Dufresne	Metzl, N.	D
320620041012	2004	10	Nath. B. Palmer	Takahashi, T. : Sweeney, C. : Sutherland, S.C.	B
353L20041230*	2005	1	L_Astrolabe	Goyet, C.	D
353L20050218*	2005	2	L_Astrolabe	Goyet, C.	D
353L20051019*	2005	10	L_Astrolabe	Goyet, C.	D
33RR20070204	2007	2	Roger Revelle	Wanninkhof, R.	D
49QB20080125	2008	2	Umitaka Maru	Hashida, G.	B
353L20090101*	2009	1	L_Astrolabe	Tilbrook, B.	B
353L20090109*	2009	1	L_Astrolabe	Tilbrook, B.	B
353L20090122*	2009	1	L_Astrolabe	Tilbrook, B.	B
353L20090218*	2009	2	L_Astrolabe	Tilbrook, B.	B
353L20090227*	2009	2	L_Astrolabe	Tilbrook, B.	B
353L20091021*	2009	10	L_Astrolabe	Tilbrook, B.	B
353L20091111*	2009	11	L_Astrolabe	Tilbrook, B.	B
353L20100219*	2010	2	L_Astrolabe	Tilbrook, B.	B
353L20100228*	2010	2	L_Astrolabe	Tilbrook, B.	B
353L20101021*	2010	10	L_Astrolabe	Tilbrook, B.	B
353L20101031*	2010	11	L_Astrolabe	Tilbrook, B.	B
09AR20110104	2011	1	Aurora Australis	Tilbrook, B.	B
353L20110220*	2011	2	L_Astrolabe	Tilbrook, B.	B
353L20110301*	2011	3	L_Astrolabe	Tilbrook, B.	B
09AR20120105	2012	1	Aurora Australis	Tilbrook, B.	A
353L20120107*	2012	1	L_Astrolabe	Tilbrook, B.	A
353L20120123*	2012	1	L_Astrolabe	Tilbrook, B.	B
353L20120218*	2012	2	L_Astrolabe	Tilbrook, B.	B
353L20120302*	2012	3	L_Astrolabe	Tilbrook, B.	B
353L20121013*	2012	10	L_Astrolabe	Tilbrook, B.	B
353L20121118*	2012	11	L_Astrolabe	Tilbrook, B.	B

74	49NZ20121128*	2012	12	Mirai	Murata, A.	A
75	353L20130110	2013	1	L_Astrolabe	Tilbrook, B.	B
76	353L20130126	2013	1	L_Astrolabe	Tilbrook, B.	B
77	353L20130219*	2013	2	L_Astrolabe	Tilbrook, B.	B
78	61TG20130202	2013	2	Tangaroa	Currie, K.I.	C
79	353L20130226*	2013	3	L_Astrolabe	Tilbrook, B.	B
80	320620140129	2014	2	Nat. B. Palmer	Takahashi, T. : Sweeney, C. : Sutherland, S.C.	D
81	09AR20141205	2015	1	Aurora Australis	Tilbrook, B.	B
82	09AR20161208	2016	12	Aurora Australis	Tilbrook, B.	A
83	09AR20161208	2017	1	Aurora Australis	Tilbrook, B.	A
84	096U20180111	2018	2	Investigator	Tilbrook, B.	A
85	49KD20181212	2019	1	Kaiyo-maru	Nomura, D.	C
86	096U20190118	2019	1	Investigator	Tilbrook, B.	B
87	09AR20191201	2019	12	Aurora Australis	Tilbrook, B.	B
88	WFCH20230214	2023	2	Le Cdt Charcot	Wanninkhof, R. : Pierrot, D.	B
89	096U20240105	2024	1	Investigator	Tilbrook, B. : Akl, J. : Neill, C.	B
90	SOCISSE *	2024	12	L_Astrolabe	Tilbrook, B. : Akl, J	N
91	SOCISSE	2025	1	L_Astrolabe	Tilbrook, B. : Akl, J	N
92	SOCISSE	2025	2	L_Astrolabe	Tilbrook, B. : Akl, J	N

93

94 (*) For these cruises discrete or underway A_T C_T data available at <https://doi.org/10.17882/102337>

95

96

97
 98
 99
 100
 101
 102
 103
 104
 105
 106
 107
 108
 109
 110
 111
 112
 113
 114
 115
 116
 117
 118
 119
 120
 121
 122
 123
 124
 125
 126
 127
 128
 129

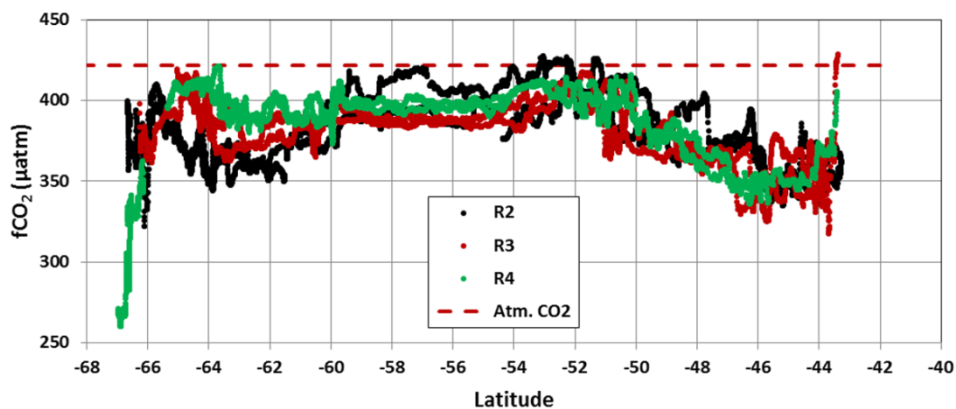
Table S2: List of cruises in the Adélie Land region (south of 63°S) from GLODAPv2.2023 (Lauvset et al, 2023, 2024) used for both surface C_T and C_{ant} estimate. The column C_{ant} identify cruises with available A_T and C_T data for C_{ant} estimates. All cruises are also used for surface data. Month indicate the season for data south of 63°S used for the trend analysis.

EXPOCODE	Year	Month	Carbon P.I.	C_{ant}
09AR19930404	1993	4	B. Tilbrook	
09AR19940101	1994	1	B. Tilbrook	
49HH19941213	1994	12	M. Ishii	Yes
09AR19941213	1995	1	M. Ishii	Yes
09AR19950717	1995	7	B. Tilbrook	
09AR19960119	1996	3	B. Tilbrook	
09AR19960822	1996	8	B. Tilbrook	Yes
09AR20011029	2001	11	B. Tilbrook	Yes
49HH20011127	2002	1	M. Ishii	
61TG20020206	2002	2	M. Ishii	
OISO-10	2003	2	N. Metzl	Yes
61TG20030217	2003	3	M. Ishii	
09AR20071216	2007	12	B. Tilbrook	Yes
09AR20080322	2008	3	B. Tilbrook	Yes
09AR20110104	2011	1	B. Tilbrook	
09AR20120105	2012	1	B. Tilbrook	
49NZ20121128	2012	12	A. Murata	
09AR20141205	2015	1	B. Tilbrook	Yes
096U20180111	2018	1	B. Tilbrook	Yes

130
131
132
133
134
135

Figure S1: Sea surface $f\text{CO}_2$ (μatm) observed in December 2024/January 2025 (R2), January-February 2025 (R3) and February 2025 (R4) along the track between Hobart and Adélie Land. In this study only data south of 63°S are used for the trend analysis. The red dashed line is the mean atmospheric CO_2 concentration in January 2025 at Cap Grim or at South Pole (422 ppm). (<https://gml.noaa.gov/dv/iadv/>).

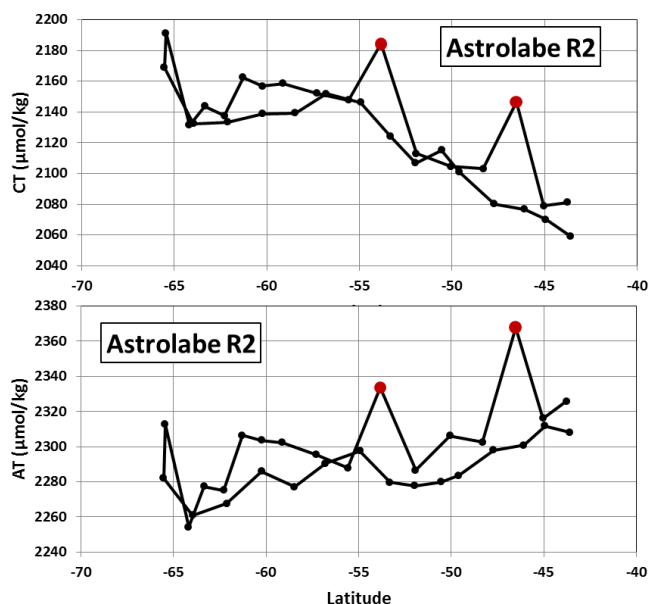
136
137
138
139
140
141
142
143
144
145
146
147
148
149
150
151



152
153
154

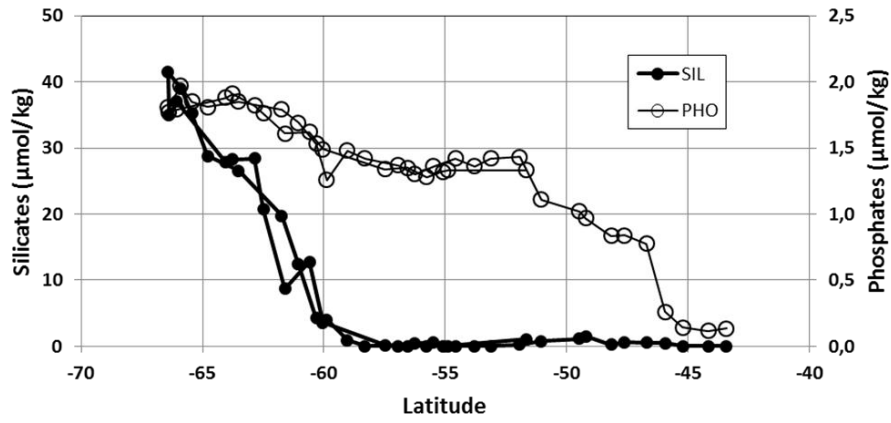
Figure S2: Sea surface A_T and C_T concentrations ($\mu\text{mol.kg}^{-1}$) observed in January 2025 along the track between Hobart and Adélie Land. The red symbols indicate suspicious data. In this study only data south of 63°S are used.

155
156
157
158
159
160
161
162
163
164
165
166
167
168
169
170
171
172
173
174
175
176
177
178
179
180



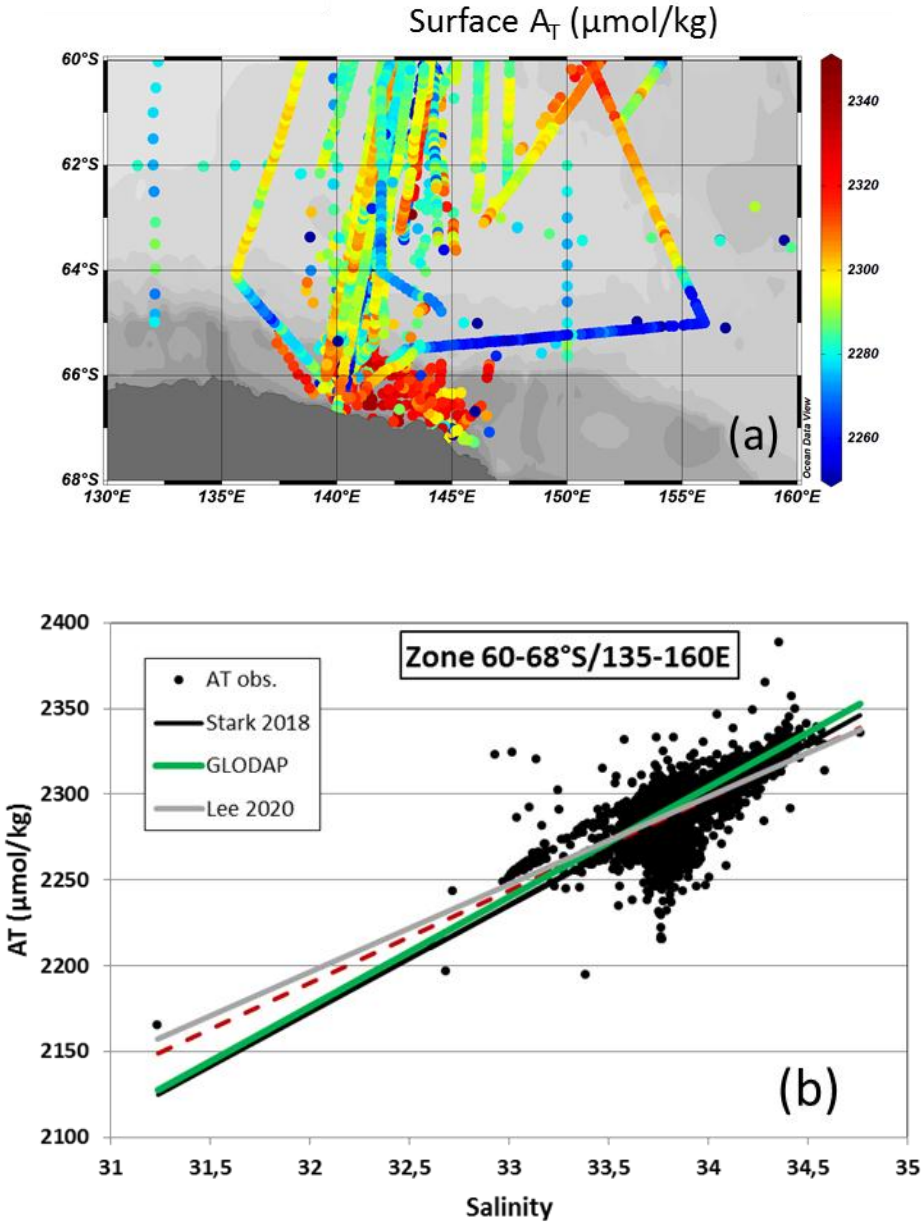
181
182
183
184
185
186
187
188
189
190
191
192
193
194
195
196
197
198
199
200
201
202

Figure S3: Sea surface silicates (black circles) and phosphates (open circles) concentrations ($\mu\text{mol.kg}^{-1}$) observed in February 2003 along the track between Hobart and Adélie Land (OISO-10 cruise). At high latitudes values for silicates of $40 \mu\text{mol.kg}^{-1}$ and phosphates of $2 \mu\text{mol.kg}^{-1}$ were used for pH and Ω_{ar} calculations using CO2sys.



203
204
205
206
207
208
209
210
211
212
213
214
215
216
217
218
219
220
221
222
223
224
225
226
227
228
229
230
231
232
233
234
235
236
237
238
239
240
241
242
243
244
245
246
247
248
249
250
251
252
253
254

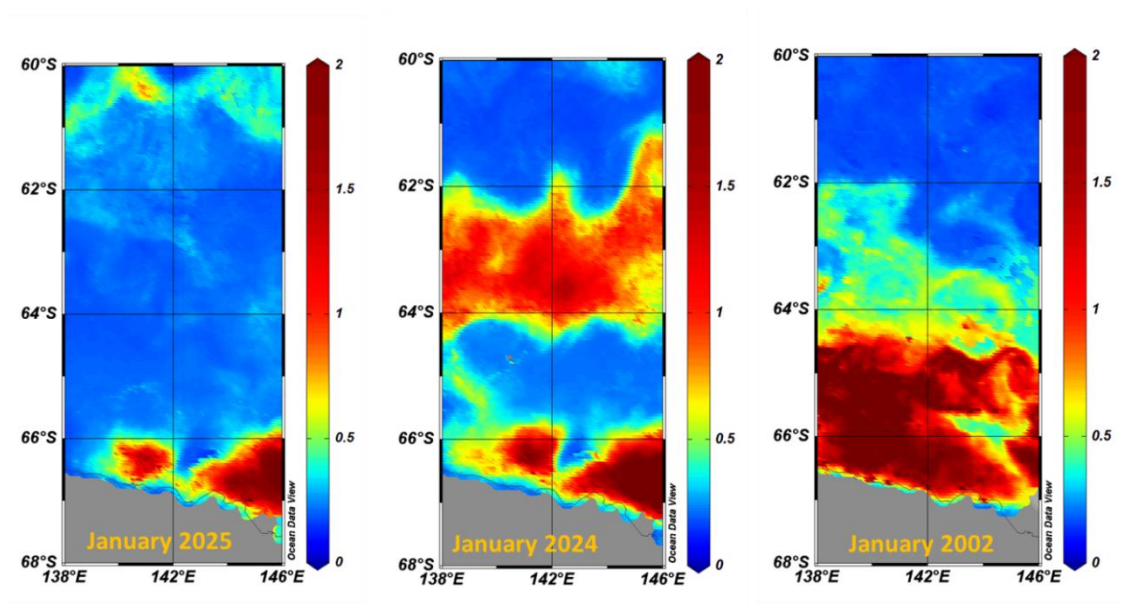
Figure S4: (a) Sea surface A_T distribution (color code in $\mu\text{mol.kg}^{-1}$) in the region from GLODAP and SNAPO-CO2 data available between 1995 and 2018. (b) A_T ($\mu\text{mol.kg}^{-1}$) versus salinity from these data and used to calculate the A_T /salinity relationship (red dashed). Also shown are the relationships from Stark et al (2018), Lee et al (2006) or using only GLODAP data (green). Figure (a) produced with ODV (Schlitzer, 2018).



255
256
257
258
259

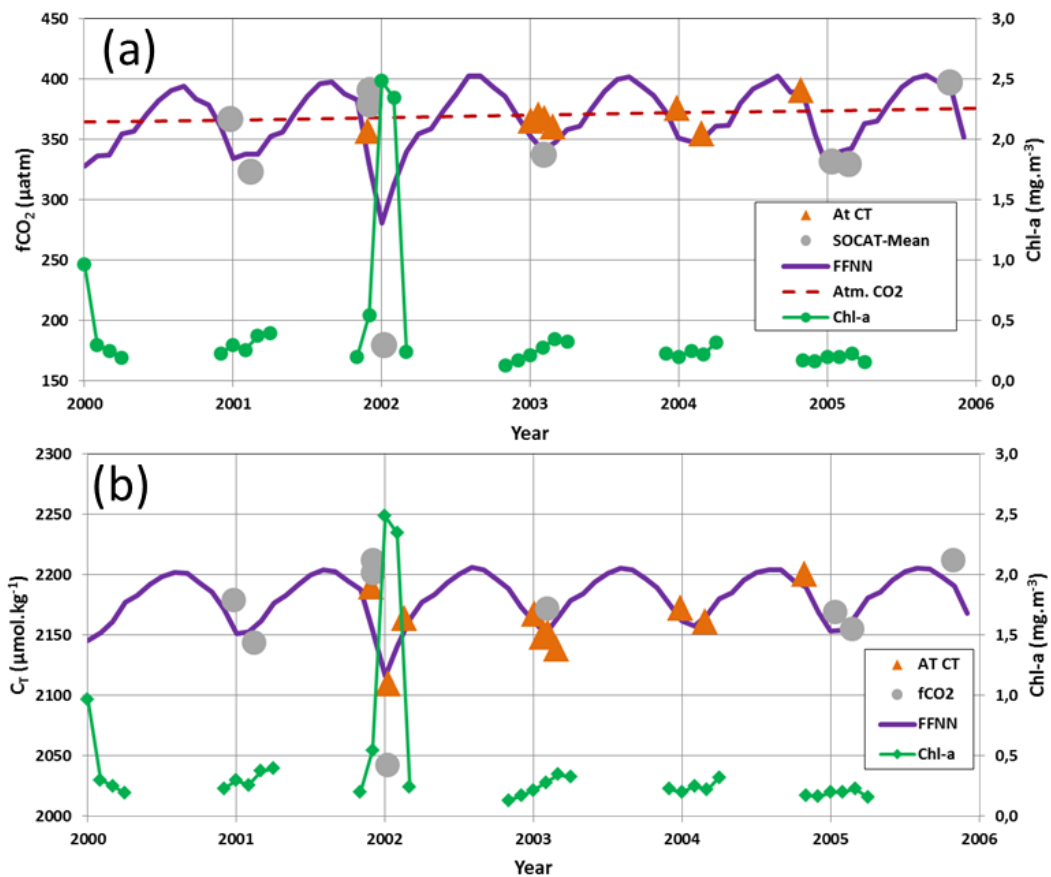
Figure S5: Maps of surface Chl-a concentration ($\text{mg}\cdot\text{m}^{-3}$) in January 2025, 2024 and 2002. Figures produced with ODV (Schlitzer, 2018) from data downloaded at <https://resources.marine.copernicus.eu/> (OCEANCOLOUR_GLO_BGC_L4_MY_009_104), last access, 29-July-2025.

260
261
262
263
264
265
266
267
268
269
270
271
272
273
274
275
276
277
278
279
280
281
282
283
284
285
286
287
288
289
290
291
292
293
294
295
296
297
298
299
300
301
302
303
304
305



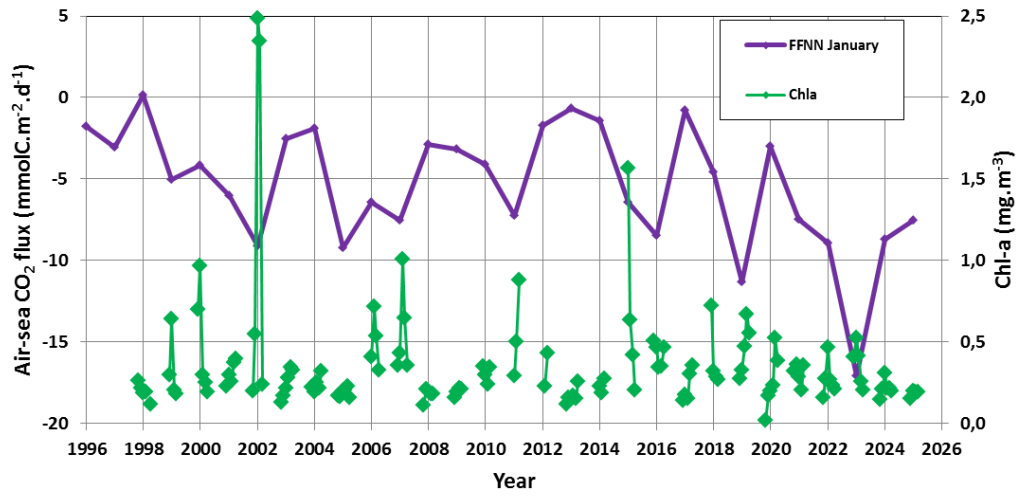
306
307
308
309
310
311
312
313
314
315
316
317
318
319
320
321
322
323
324
325
326
327
328
329
330
331
332
333
334
335
336
337
338
339
340
341
342
343
344
345
346
347
348
349
350
351
352
353
354
355
356
357

Figure S6: Same as figure 6 for the period 2000-2006 to highlight the anomaly in 2002. Time-series of (a) sea surface $f\text{CO}_2$ (μatm) and (b) C_T ($\mu\text{mol.kg}^{-1}$) observed south of 65°S based on SOCAT $f\text{CO}_2$ data in summer (grey circles) and from $A_T C_T$ data in summer (orange triangles) Also shown are the monthly values of the FFNN model (purple) and Chl-a concentrations (green, mg.m^{-3}) at the same location. The red line in (a) is the atmospheric $f\text{CO}_2$.



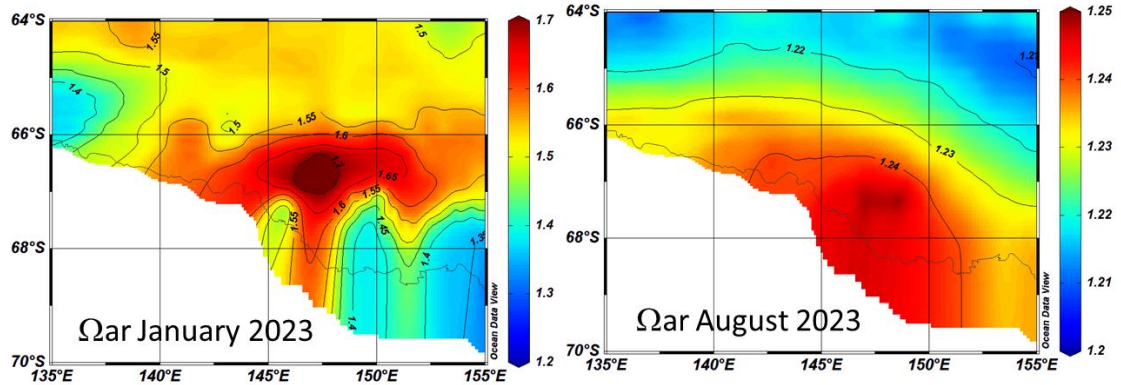
358
359
360
361
362
363
364
365
366
367
368
369
370
371
372
373
374
375
376
377
378
379

Figure S7: Time-series of air-sea CO₂ fluxes (mmolC.m⁻².d⁻¹) in January 1996-2025 from the FFNN model (centered at 65°S-140°E) and of the Chl-a concentrations (green, mg.m⁻³) at the same location. When Chl-a was high (e.g. 2002, 2015) the ocean was a stronger CO₂ sink.



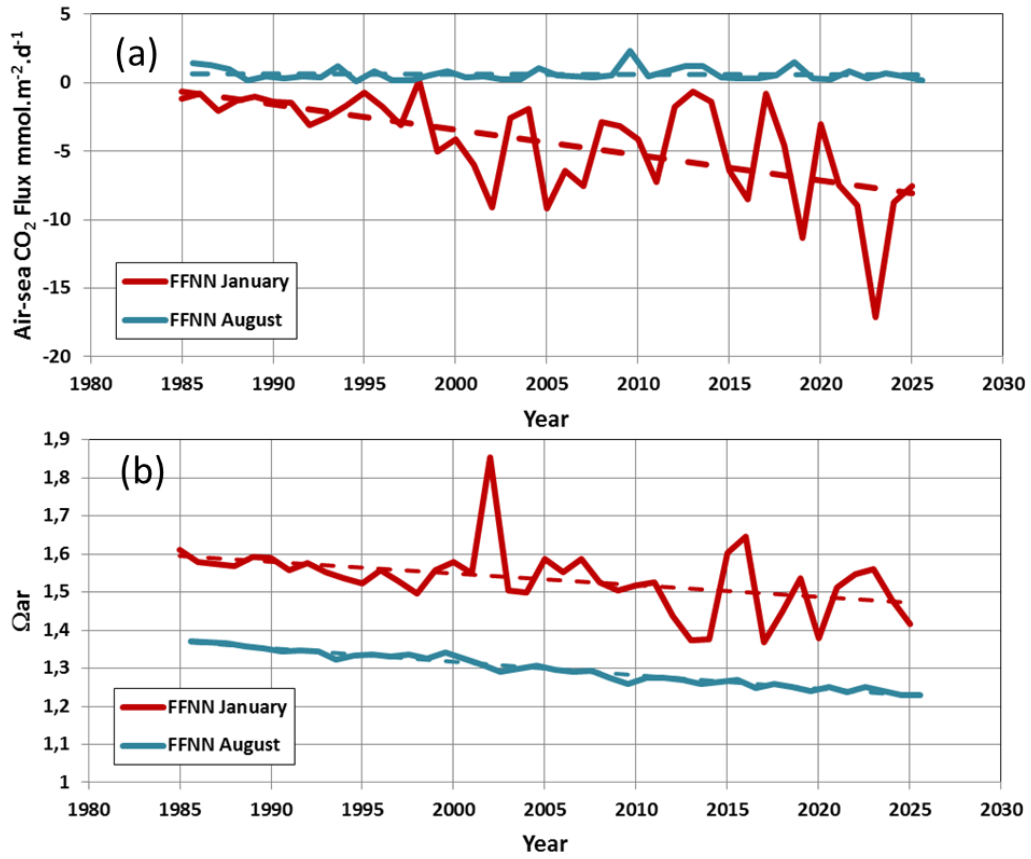
380
381
382
383
384
385
386
387
388
389
390
391
392
393
394
395
396
397
398
399
400
401
402
403
404
405
406
407
408
409
410
411

Figure S8: Maps of Ω_{ar} in January 2023 (left) and August 2023 (right) in the Adélie Land region based on the FFNN model. Note the different scales. During austral winter $\Omega_{ar} < 1.3$. In summer Ω_{ar} presents high variability linked to biological processes. Figures produced with ODV (Schlitzer, 2018).



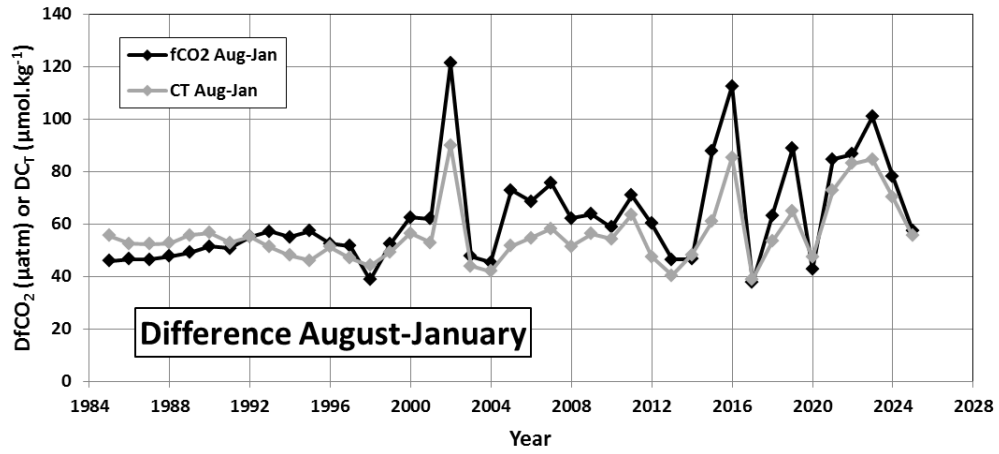
412
413
414
415
416
417
418
419
420
421
422
423
424
425
426
427
428
429
430
431
432
433
434
435
436
437
438
439
440
441
442
443
444

Figure S9: Time-series of (a) air-sea CO₂ fluxes (mmolC.m⁻².d⁻¹) and (b) Ω_{ar} in 1985-2025 from the FFNN model (centered at 65°S-140°E) in January (red) and August (blue). Dashed lines are the trends for each season (see Table 3). Here, we highlight the variability in austral summer.

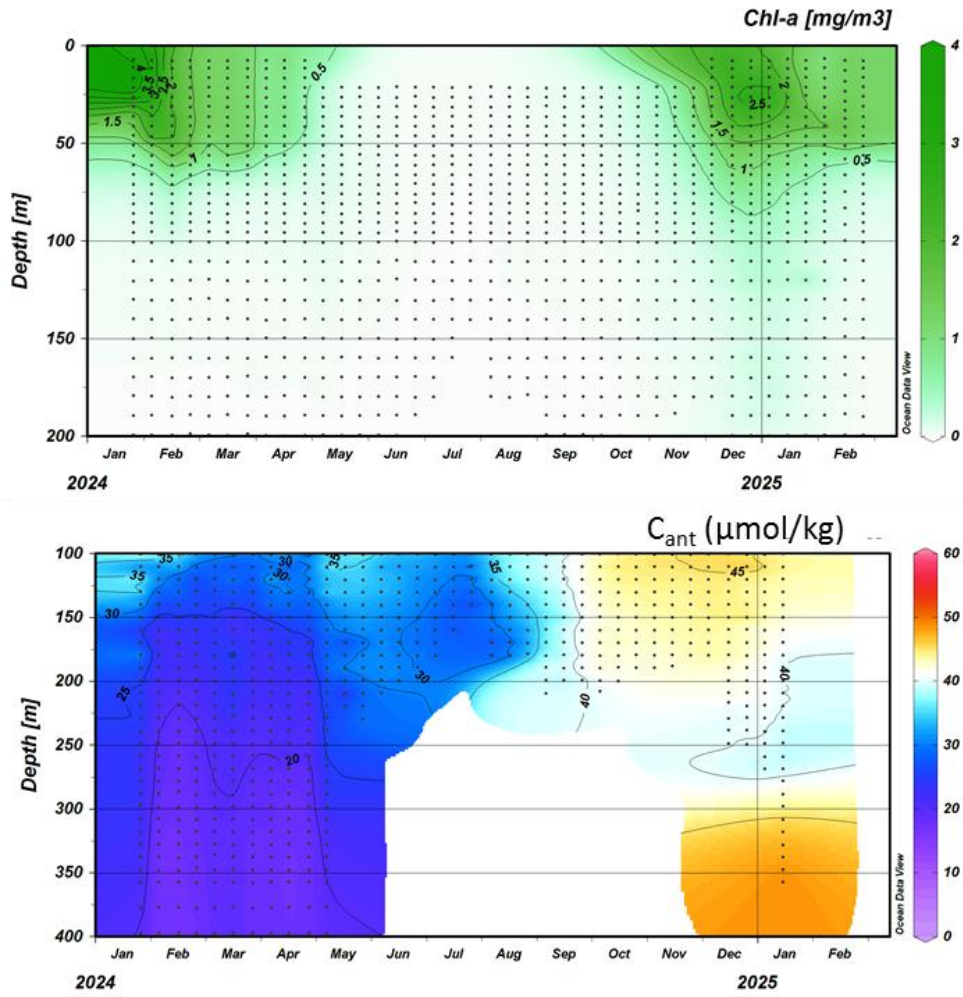


445
446
447
448
449
450
451
452
453
454
455
456
457
458
459
460
461
462
463
464
465
466
467
468
469
470

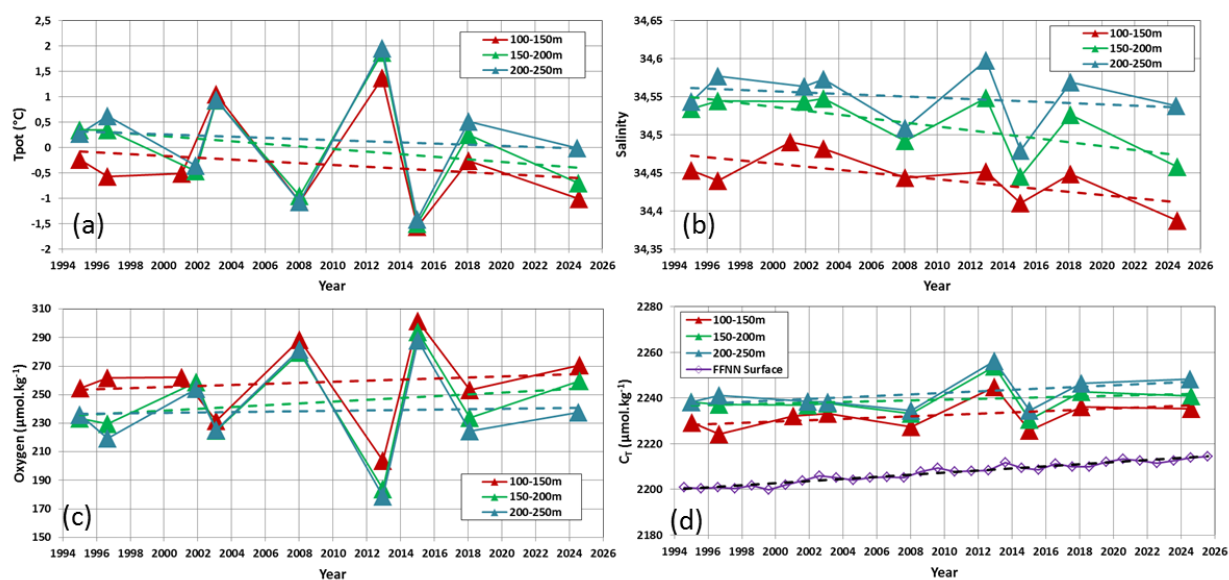
Figure S10: Time-series of the seasonal difference (August-January) for $f\text{CO}_2$ and C_T based on the FFNN model (centered at 65°S - 140°E). The differences present high variability starting in 1998 when the model is constrained by Chl-a satellite data. No significant trends were observed but the seasonal amplitude was variable around 2000-2008 and 2015-2023.



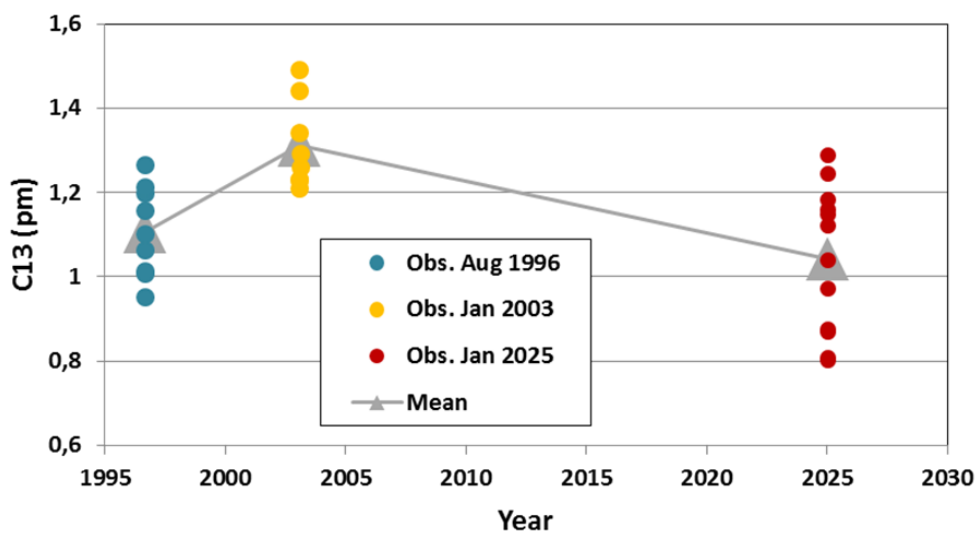
471
472 Figure S11: Time-series of Chl-a concentrations ($\text{mg}\cdot\text{m}^{-3}$) and C_{ant} ($\mu\text{mol}\cdot\text{kg}^{-1}$) derived from the BGC-
473 Argo float (WMO 2903867) from January 2024 to February 2025. The C_{ant} concentrations are
474 estimated below 100m and only for good pH_T data (Jan-2024/Jan-2025). Dots indicate the location of
475 data. Figures produced with ODV (Schlitzer, 2018).
476



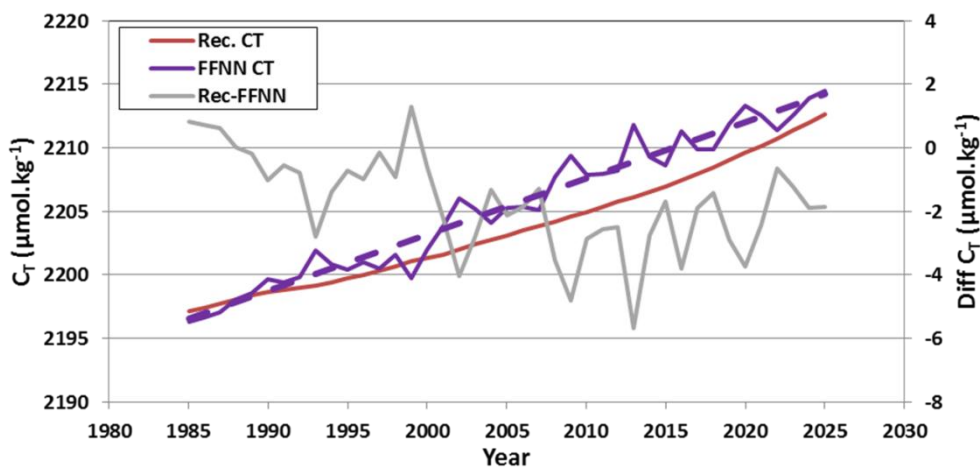
523
 524 Figure S12: (a): Time-series of (a) Potential temperature ($^{\circ}\text{C}$), (b) salinity, (c) Oxygen ($\mu\text{mol.kg}^{-1}$) and
 525 (d) C_T ($\mu\text{mol.kg}^{-1}$) observed in 3 layers (below 100m) from 1994 to 2024. The trends are represented
 526 by dashed lines (see Table 4). In (d) are also shown the C_T concentrations in surface in August from
 527 the FFNN model (purple and dashed purple line is the C_T trend of $0.46 \mu\text{mol.kg}^{-1}.\text{yr}^{-1}$). In 2013 an
 528 anomaly is identified for all properties in subsurface and sea surface C_T from the FFNN model is also
 529 slightly higher in 2013.
 530
 531
 532



540
 541
 542
 543
 544
 545
 546
 547
 548
 549
 550
 551 Figure S13: Sea surface $\delta^{13}\text{C}$ (per mill) observed in August 1996, January 2003 and January 2025
 552 south of 62°S in the Adélie Land region. The decrease of $\delta^{13}\text{C}$ from 2003 to 2025 (same season) of -
 553 0.27 on average is linked to the anthropogenic CO_2 uptake (i.e. a Suess effect of $-0.0123.\text{yr}^{-1}$).
 554
 555



575 Figure S14: Time-series of C_T concentrations ($\mu\text{mol.kg}^{-1}$) based on the FFNN model (purple) and the
 576 reconstruction for August using C_{ant} fitted (C_{ant} fit, red line, see Eq. 2,) and their difference (grey right
 577 axis). The dashed line is the FFNN trend ($0.44 \mu\text{mol.kg}^{-1}.\text{yr}^{-1}$).
 578
 579
 580



581
582
583
584
585
586
587
588
589
590
591
592
593
594
595
596
597
598
599
600
601
602
603
604
605
606
607
608
609
610
611